Asian Journal of Chemistry; Vol. 25, No. 17 (2013), 9617-9621

ASIAN JOURNAL OF CHEMISTRY

http://dx.doi.org/10.14233/ajchem.2013.15101

# Preparation and Electrical Properties of Mn-Doped $Ba_{1-x}Sr_xTiO_3$ Ceramic Powder

KEYAN HU, JUNSHENG LIU* and MENG LI

Key Laboratory of Membrane Materials & Processes, Department of Chemical and Materials Engineering, Hefei University, 99 Jinxiu Road, Hefei Economic and Technological Development Zone, Hefei 230601, P.R. China

*Corresponding author: Fax: +86 551 62158437; Tel: +86 551 62158439; E-mail: jsliu@hfuu.edu.cn

(*Received*: 7 January 2013; *Accepted*: 7 October 2013) AJC-14240

Mn-doped $Ba_{1-x}Sr_xTiO_3$ (BST) ceramic powder had been successfully prepared by sol-gel process. The formation process of $Ba_{0.4}Sr_{0.5}Mn_{0.1}TiO_3$ (BSMT) was tested through thermal analysis (TG-DTA) and X-ray diffraction. The electrical properties and microstructure of Mn-doped BST showed that manganese, which was doped at the A-site of $ABO_3$ perovskite materials, could not affect the perovskite phase structure, but could influence the resistance voltage characteristics in low frequency and the resistance value was lowered from 10381-1076 kΩ, about 10 times decline. The relationship between resistance and temperature exhibited that in middle frequency, the sample displayed double peak effect and the electrical characteristics related to ferroelectricity of grains and shifted from high temperature to low temperature with an increasing frequency. But in low frequency, it revealed the characteristics of resistance and capacitance of grains. These phenomena could be interpreted by Heywang model theory.

**Key Words: $Ba_{1-x}Sr_xTiO_3$ (BST), Mn-Doped, Sol-gel, Resistance characteristics.**

## INTRODUCTION

Since the report that ferroelectric materials can be used to fabricate large scale integrated circuit (VLSI) memory, Post-Gbit dynamic random access memory (DRAM) capacitors prepared *via* ferroelectric materials have attracted considerable attentions in recent years. Barium strontium titanate [($Ba_{1-x}Sr_xTiO_3$), (BST)] is an attractive capacitor material for dynamic random access memories and infrared detectors due to its chemical stability, excellent structure and dielectric properties compared to other ferroelectric materials such as $BaTiO_3$, $PbTiO_3$, *etc.*[1-6].

$BaTiO_3$ and $SrTiO_3$ are representative $ABO_3$ model perovskite materials and $Ba_{1-x}Sr_xTiO_3$ (BST) is also a solid solution system between $BaTiO_3$ and $SrTiO_3$, *i.e.*, $Ba_{1-x}Sr_xTiO_3$ simultaneously has the advantages of the high dielectric constant of $BaTiO_3$ and the structural stability of $SrTiO_3$. At room temperature, it is known that the solid solution system is in a ferroelectric phase when Ba content 1-x is in a range from 0-0.7[7,8]. Furthermore, the electrical properties of BST such as dielectric constant, dielectric loss, depend upon the composition, dopant, microstructure, *etc*. and the electrical properties and kinetic behaviours of undoped and doped BST have been fully investigated[3,7,9,10]. However, the characterizations of doped BST, especially manganese, which has an influence on the grain boundary resistance[11-13], have been insufficiently investigated. It is concluded that dopant can significantly modify the dielectrical and electrical properties of ferroelectric materials such as barium strontium titanate (BST), lead zirconate titanate (PZT), *etc*. Some researchers have studied the properties of donor for the B site of $ABO_3$ perovskite structure materials, for example Jiang *et al.*[14,15] has researched the defect structure and electrical property of B-site doped $ABO_3$ perovskite structure material, $Ba_{0.5}Sr_{0.5}Co_{0.8}Fe_{0.2}O_{3-\delta}$ and Kim[9] also studied the lower leakage current and dielectric loss of a donor for the B site perovskite structure. However, the investigation of donor for the A site of $ABO_3$ perovskite structure materials is relatively insufficient.

Barium strontium titanate (BST) or $BaTiO_3$ has been prepared by a variety of different techniques, for example Xu *et al.*[5] prepared nanosized $BaTiO_3$ powders by hydrothermal method; but among them, sol-gel process is probably the most prominent one, because it offers some significant merits such as purity, homogeneity and low reaction temperature that cannot be obtained by other methods. The simplicity also make it an excellent technique for manufacturing other $BaTiO_3$-base novel materials, for instance Wei *et al.*[16] prepared Pan/$BaTiO_3$ nanocomposite by sol-gel technique.

In our previous investigation, the kinetic parameters of $Ca^{2+}$ and $Mn^{2+}$ co-doped $Ba_xSr_{1-x}TiO_3$ to prepare $Ba_{0.4}Sr_{0.5}Ca_{0.08}Mn_{0.02}TiO_3$ solid solution have been studied[10,11]. The main purpose of present work is to investigate the effect of resistance temperature and direct current (DC) bias voltage

at different frequencies, which are crucial to the dynamic random access memories capacitors, on the electrical properties of Mn-doped BST ceramic powder. Special attention will be given to the influence of the cationic substitution of Mn in A-site such as Ba or Sr site of the $ABO_3$ perovskite structure on electrical properties of barium strontium titanate ceramic powder prepared by sol-gel process.

## EXPERIMENTAL

**Preparation of sample powders:** $Ba_{1-x}Sr_xTiO_3$ (x = 0.5) was selected as standard compound (undoped BST) for simplicity.

All sol-gel reactions were performed at room temperature unless otherwise noted. The samples were prepared by mixing 0.4 mol % $Ba(OH)_2 \cdot 8H_2O$ and 0.5 mol % $Sr(OH)_2 \cdot 8H_2O$ and 0.1 mol % $Mn(CH_3COO)_2 \cdot 4H_2O$ was added to the basic composition, then all dissolved by glacial acetic acid to form homogeneous drop solution. While the precursor that was fabricated from tetrabutyl titanate [$Ti(OC_4H_9)_4$] in the presence of *n*-butanol was stirred for additional 0.5 h. Finally, the homogeneous drop solution was added dropwise into the precursor over 2 h. The resulting mixture was drastically stirred *via* magnetic stirrer for additional 2 h and allowed to stand. After completion, a deeply yellow coloured gel was formed within 6 h and left for 7 days at 70 ºC. Then, the xerogel was sintered at 500, 650, 750 and 850 ºC for 2 h in air to prepare ceramic powder, respectively. The undoped BST sample was manufactured as the same procedure.

**Powder characterizations:** The xerogel was characterized using thermogravimetric analysis and differential thermal analysis (WCT-2A, Beijing optical instrument Co.) at a heating rate of 10 ºC/min in dry air atmosphere from room temperature to 900 ºC.

To study the phase development with increasing calcinations temperature in the samples, the xerogels were sintered in air atmosphere at various temperatures for 2 h, up to 850 ºC. Powder X-ray diffraction (XRD) measurements were performed on a diffractometer (D/max-γ B, Japan) using an copper anticathode (wavelength $CuK_\alpha$: 0.15406 nm).

For electrical contact, the flat surfaces of the samples were coated with Ag alloy rubbing; DC resistivity of these samples was measured at room temperature *via* two-probe method. The frequency dependence of impedance was determined by an impedance analyzer (ZL5 intelligence LCR, Shanghai) in the frequency range of 0.5-100 kHz and the DC bias voltage dependence of impedance was measured by the same impedance analyzer within the range of 0-25 voltage. DC bias voltage was provided through manostat (PPE-3323, Goodwill, Taiwan).

## RESULTS AND DISCUSSION

**TG-DTA analysis:** The TG-DTA analysis was carried out on WCT-2A apparatus at a heating rate of 10 ºC/min under a dry air atmosphere, heated up to 900 ºC and the result was shown in Fig. 1.

From the TG plot, a three-stage weight loss could be seen, namely, a steady weight loss over the temperature range from 42-281 ºC and a sharp fall in specimen weight over the temperature range from 281 to 570 ºC. Further weight loss was also observed at temperature above 570 ºC. The weight loss at temperatures below 280 ºC was believed to be due to the elimination of residual water and the organic components in the gel. The sharp fall weight loss in specimen over the temperature range from 281-570 ºC was related to the decomposition of the acetic acid, the group of tetrabutyl as well as *n*-butanol. Further weight loss beyond 570 ºC implied the completion of all the reactions involving a weight loss.

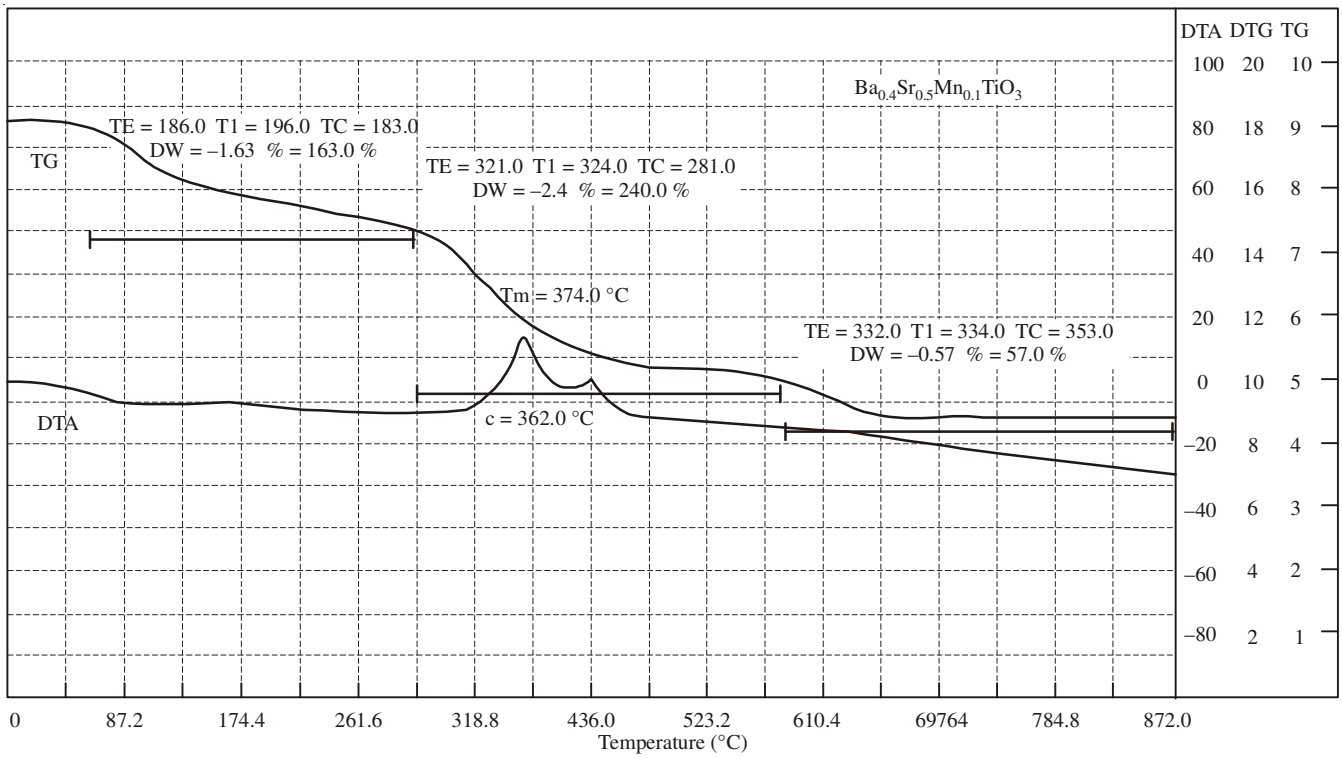


Fig. 1. TG-DTA curves at a heating rate of 10 ºC/min

As illustrated in DTA curve, no other exothermic or endothermic peak was observed except in the range from 281-570 ºC, indicating no other compounds except Mn-doped BST ($Ba_{0.4}Sr_{0.5}Mn_{0.1}TiO_3$) was formed in the process of annealing. This result was in agreement well with the TG curve and XRD patterns (as shown in Fig. 2 hereinafter). The maximum exothermic peak in DTA curve at 374 ºC resulted from the formation of crystalline of Mn-doped BST. The weight loss was summarized in Table-1.

TABLE-1
THERMOGRAVIMETRIC ANALYSIS OF SAMPLE IN TGA CURVES

| Temperature range (ºC) | Weight loss (mg) |
|---|---|
| 42–281 | 1.63 |
| 281–570 | 2.40 |
| 570–872 | 0.57 |

**XRD analysis:** Fig. 2 presented the XRD patterns of the Mn-doped BST powder annealed at different temperatures. It was clear that when the temperature was lower than 500 ºC (Fig. 2a), the powder was amorphous and the crystallization began at *ca.* 500 ºC. The intensities of diffraction peaks, which are related to the degree of the completion of the phase and crystallinity improved, were enhanced with increase of the annealing temperature, meanwhile the peak locations such as (110), (111), (200), (211) and (220) remained constantly (Fig. 2b-d), indicating an increase in crystalline. Because of no pattern in JCPDS [Joint Committee on Powder Diffraction Standards file], the pattern of samples exhibited similar XRD patterns with standard compound, $Ba_{0.5}Sr_{0.5}TiO_3$ [pattern 39-1395 file] and the major peak locations, (110), (111), (200), (211) and (220) were all identical, implying that corresponding to the BST perovskite structure was still obtained after $Mn^{2+}$ substituting A-site $Ba^{2+}$. This was attributed that the small amount of Mn ion could not lead to large oxygen vacancy even though $Mn^{2+}$ ionic radius (0.083 nm) is smaller than that of $Ba^{2+}$ (0.135 nm), $Sr^{2+}$ (0.118 nm), $O^{2-}$ (0.14 nm)[17,18]. In addition, no peak splitting was observed on the X-ray diffraction pattern for sample gels calcined at temperature ranging from 650-850 ºC, implying that the crystalline form of sample was still single phase at this temperature range. The result was also confirmed by TG-DTA curves (Fig. 1).

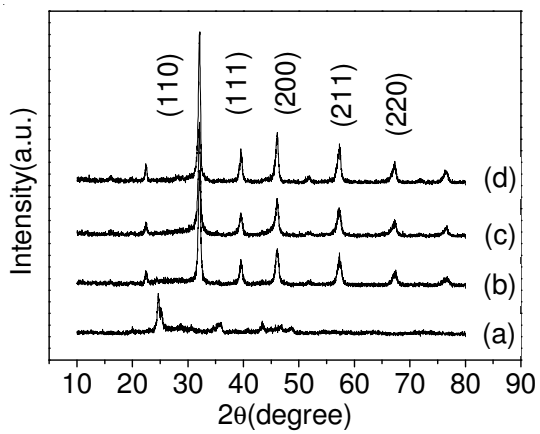


Fig. 2. XRD patterns of sample calcined at various temperatures. (a) 500 ºC, (b) 650 ºC, (c) 750 ºC, (d) 850 ºC

**Resistance voltage characteristics:** The investigation of the DC electric field dependence of the capacitance is one of the most useful methods of gaining insight into the behaviours of ferroelectric materials[19,20]. The DC field dependence of the samples was investigated by measuring resistance voltage (R-V) characteristics. The R-V characteristics of both Mn-doped and undoped BST sample powders at room temperature were shown in Fig. 3. From the R-V figures, it is interesting to find that different behaviours were observed in low frequency such as at 1 and 5 kHz; namely, there were upward tendencies for the Mn-doped BST (Fig. 3b), whereas horizontal trends for undoped BST (Fig. 3a). However, resemble behaviours had been illustrated in majority of high frequency such as 20-100 kHz for both samples. These might be attributed to the frequency and field dependence of the ferroelectric properties of the samples.

Generally, $Mn^{2+}$ (0.083 nm) has similar ionic radius with titanate ion (0.061 nm)[18] and Mn-doped $Ba_{1-x}Sr_xTiO_3$ can enhance the positive temperature coefficient (PTC) effect of BST sample[12]. On the one hand, if Ti site is substituted by Mn ion, holes or cationic vacancies will be appeared. The deficit compensation mechanism was followed as[21]:

$$MnO + BaO + 0.5O_2 \rightarrow Ba_{Ba}^{\bullet} + Mn_{Ti}^{\bullet} + 3O_o^{\bullet} + 2h^{\bullet} \quad (1)$$

$$MnO + BaO \rightarrow Ba_{Ba}^{\bullet} + Mn_{Ti}^{\bullet} + 2O_o^{\bullet} + Vo^{\bullet} \quad (2)$$

On the other hand, according to ion polarization theory[22], the static polarizability of materials can be described as:

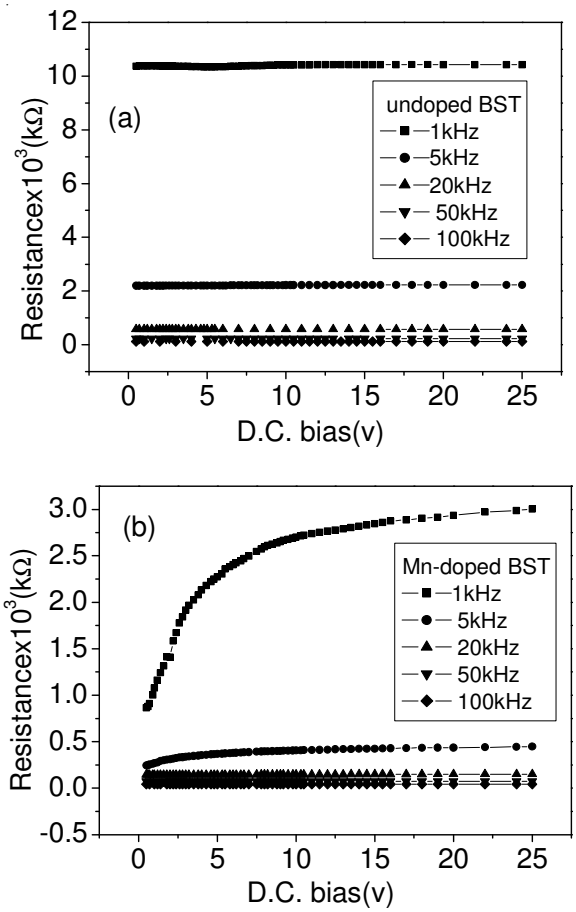


Fig. 3. Resistance-voltage (R-V) characteristics of BST powders at room temperature, (a) undoped BST, (b) Mn-doped BST

$$X_e = \frac{e^2}{\varepsilon_0 m}\sum_q \frac{1}{\omega_q^2} \quad (3)$$

the dynamic polarizability of materials can be described as:

$$X'_e = \frac{e^2}{\varepsilon_0 m}\sum_q \frac{1}{\omega_q^2 - \omega^2} \quad (4)$$

where $\omega_q$ is the intrinsic frequency of the qth polarization charge of sample, m is the effective mass of polarization charge, $\varepsilon_0$ is the vacuum dielectric constant, e is the polarization charge and $\omega$ is the frequency of applied field.

As described in eqns. 3 and 4, it is obvious that the dynamic polarization elevated with an increasing frequency in applied field. As a result, it caused an increase in the resistances of both doped and undoped BST. At low frequency, the roles of spontaneous polarization and static polarization were the dominant form for both doped and undoped BST and semiconducting behaviour was not significant. Manganese existed in the grain boundary and blocked the thermal motion of electrons. But in high frequency, dynamic polarization would gain an advantage over the static polarization in the applied field and the spontaneous polarization could be neglected due to its small value compared to the large one of dynamic polarization, meanwhile semiconducting behaviour was elevated. As a result, the resistance was considerably decreased and the effective charge density of electrons and conductivity would be promoted with the increasing frequency. Consequently, the resistances tended to become stable with the increasing frequency. On the other hand, the resistance of Mn-doped BST was significantly decreased in comparison with that of undoped BST owing to the substitution of A-site, which caused the holes or oxygen vacancies (as expressed in eqns. 6 and 7 hereinafter) and ion polarization. For example, the resistance value was lowered from 10381 kΩ (undoped BST, 1 kHz, 1v DC bias voltage, Fig. 3a) to 1076 kΩ (Mn-doped BST, 1 kHz, 1v DC bias voltage, Fig. 3b), about 10 times decline.

**Resistance temperature characteristics:** The relationship between resistance and temperature *versus* frequency was presented in Fig. 4. It indicated that the resistance and temperature (R-T) curves of Mn-doped BST samples decreased rapidly with the increasing temperature, which exhibited negative temperature coefficient (NTC) effect in both low frequency (Fig. 4a-d) and high frequency (Fig. 4g-h), *i.e.*, f = 0.5-10 kHz and f = 66.66-100 kHz, respectively. But in middle frequency (Fig. 4e-f), *i.e.*, f = 20-50 kHz, the resistance and temperature curves displayed double peak effect and the sites of double peak were shifted from high temperature to low temperature as the frequency elevated, namely, they changed from 85 ºC (105.77 kΩ) and 280 ºC (99.66 kΩ) at 20 kHz to 60 ºC (3.8 kΩ) and 155 ºC (3.97 kΩ) at 50 kHz, respectively. These phenomena could be interpreted by Heywang model theory described as below[23].

According to Heywang model theory, the resistance of materials was determined by grain boundary potential barrier and temperature, doping method could change the resistance of materials within certain temperature. The relationship between the resistance and temperature can be described by eqn. 5[24]:

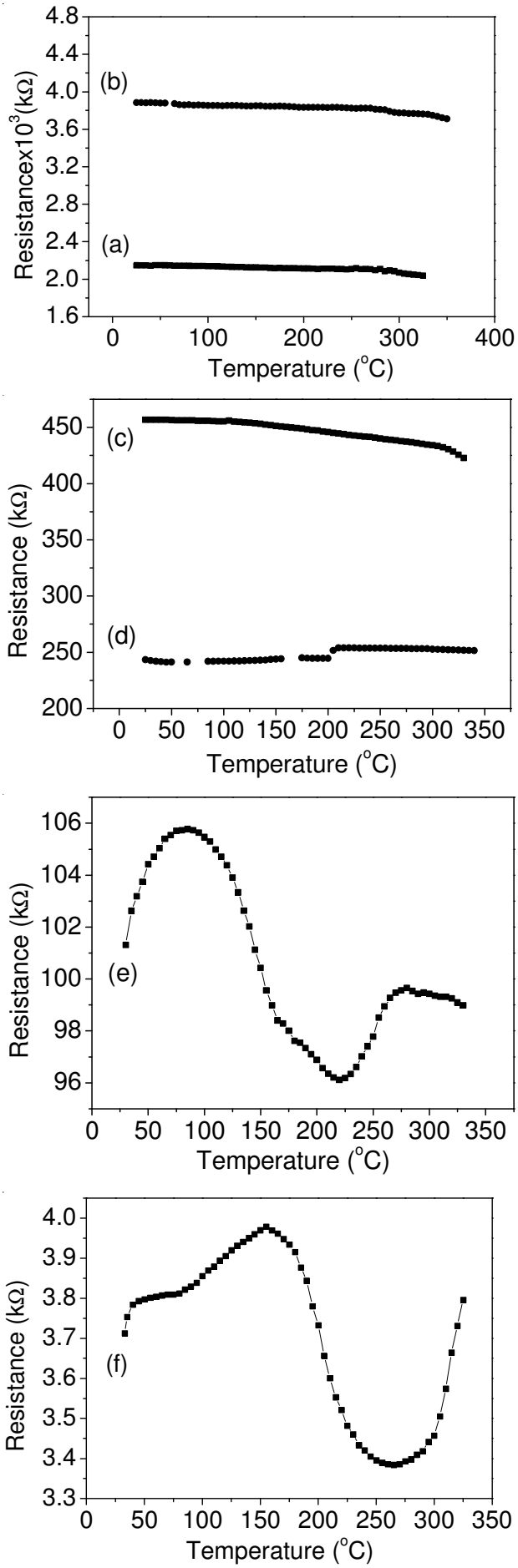

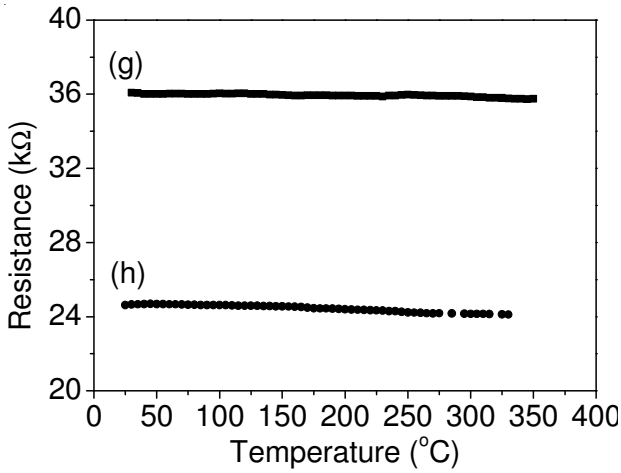


Fig. 4. Relationships between resistance and temperature of Mn-doped BST at different frequencies, (a) 0.5 kHz, (b) 1 kHz, (c) 5 kHz, (d) 10 kHz, (e) 20 kHz, (f) 50 kHz, (g) 66.66 kHz, (h) 100 kHz

$$\rho = B\exp\left(\frac{e\Phi}{kt}\right) \quad (5)$$

where B is certain constant, k is Boltzmann constant, Φ is the grain boundary potential barrier and e is the charge capacity of electron, t is the temperature.

It is evident that the resistance is determined by the grain boundary potential barrier Φ and temperature t. When the temperature increased, grain boundary potential barrier might increase dramatically, as a result, the resistance escalated drastically because the motion of electrons was prevented in grain boundary. In middle frequency, the properties of R-T exhibited the electrical characteristics related to ferroelectricity of grains. But in low frequency, it revealed the characteristics of resistance and capacitance of grains[25].

Moreover, it is well known that the positive temperature coefficient effect stems from the grain boundaries of BST. It has been well reported that the positive temperature coefficient effect depends on the extent of oxidation, that is, the production and diffusion of the oxygen vacancies are important in the formation of positive temperature coefficient effect[12,17,26].

At the grain boundary and in the grain, the formation of oxygen vacancies is expressed as follows[12]:

$$Mn_2O_3 \rightarrow 2Mn_{Ti}^{\bullet} + V_o^{\bullet\bullet} + 3O_o^{\times} \quad (6)$$

$$2Mn \rightarrow 2Mn_{Ti}^{\bullet\bullet} + 2V_o^{\bullet\bullet} + 2O_o^{\times} \quad (7)$$

Obviously, $Mn^{3+}$ dissolved in the grain boundary more quickly than in the bulk of the grain at an oxidizing atmosphere. Compared with the undoped sample of barium strontium titanate, the partial replacement of Mn ion at A-site favoured a decrease in resistance in both low and high frequency; whereas in middle frequency, the number of hopping electrons increased with an elevated temperature, which greatly weakened the influence of dopant Mn ion[24] and ion polarization also tended to be stable so that the sites of double peak were shifted to low temperature. Furthermore, manganese possessed changeable valent, which was also responsible for the abnormal change in resistance of Mn-doped barium strontium titanate ceramic powder.

In summary, the interaction of grain boundary potential barrier and temperature lead to double peak effect in Mn-doped barium strontium titanate sample in middle frequency.

## REFERENCES

1. Y. Miyasaka and S. Matsubara, in Proceedings of the 7th International Symposium on Application of Ferroelectrics (IEEE, Piscataway, NJ, 1991), p. 121 (1990).
2. M. Viviani, M.T. Buscaglia, V. Buscaglia, L. Mitoseriu, A. Testino and P. Nanni, In Proceedings of the 13th IEEE International Symposium on Applications of Ferroelectrics, p. 103 (2002).
3. Q. Yin, M. Ding, Y. Zhou, C. Tian, H. Lu and D. Zhao, *Asian J. Chem*., **24**, 4095 (2012).
4. K.K. Raina, P. Kumar and G. Sumana, *Asian J. Chem*., **18**, 3384 (2006).
5. V.N. Shut, S.R. Syrtsov and V.L. Trublovsky, *Phys. Solid State*, **53**, 1859 (2011).
6. X.H. Zhu, E. Defaÿ, B. Guigues, G. Le Rhun, C. Dubarry and M. Aïd, *J. Eur. Ceram. Soc*., **30**, 471 (2010).
7. W. Zhang, Z. Xu, C. Wang and B. Zhao, *Mater. Res. Bull*., **38**, 133 (2003).
8. K. Abe and S. Komatsu, *J. Appl. Phys*., **77**, 6461 (1995).
9. K.-T. Kim and C.-I. Kim, *Microelectron. Eng*., **66**, 835 (2003).
10. S.F. Liu, J.S. Liu, X.Z. Han and X.F. Zhang, *Chem. Online*, **67**, w030 (2004).
11. J.S. Liu and G.N. Fan, *Chin. J. Chem. Phys*., **19**, 367 (2006).
12. Q. Jianquan, G. Zhilun, W. Yajing and L. Longtu, *Mater. Chem. Phys*., **73**, 97 (2002).
13. J. Zhang, J. Zhai and X. Yao, *Scr. Mater*., **61**, 764 (2009).
14. G.S. Jiang, C.L. Song, D.C. Li, S.J. Feng, W. Liu and C.S. Chen, *Chin. J. Chem. Phys*., **17**, 75 (2004).
15. D. Czekaj, A. Lisinska-Czekaj, T. Orkisz, J. Orkisz and G. Smalarz, *J. Eur. Ceram. Soc*., **30**, 465 (2010).
16. J.H. Wei, J.G. Guan, J. Shi and R.Z. Yuan, *Chin. J. Chem. Phys*., **16**, 401 (2003).
17. C. Lemoine, B. Gilbert, B. Michaux, J.-P. Pirard and A. Lecloux, *J. Non-Cryst. Solids*, **175**, 1 (1994).
18. R.D. Shannon, *Acta Crystallogr. A*, **32**, 751 (1976).
19. T. Zhang and H. Ni, *Sens. Actuators A*, **100**, 252 (2002).
20. K. Sreenivas, A. Mansingh and M. Sayer, *J. Appl. Phys*., **62**, 4475 (1987).
21. Z.T. Zhang, M. Qing and H.F. Sun, *J. Funct. Mater*., **29**, 366 (1998).
22. D.M. Zhang, P. Zheng, X.D. Wang, Z.J. Chen, X.Y. Zhang, D.Z. Wang and D.S. Xu, *J. Funct. Mater*., **30**, 509 (1999).
23. W. Heywang, *Solid-State Electron*., **3**, 51 (1961).
24. X.D. Wang, D.M. Zhang, Z.J. Chen, P. Zheng, X.Y. Zhang, D.Z. Wang and D.S. Xu, *J. Funct. Mater*., **30**, 512 (1999).
25. X.D. Yu and G.R. Li, *J. Inorg. Mater*., **12**, 375 (1997).
26. M. Kuwabara, *Solid-State Electron*., **27**, 929 (1984).